Published in final edited form as:
Lasers Surg Med. 2010 December ; 42(10): 716–727. doi:10.1002/lsm.21009.

Pilot clinical study for quantitative spectral diagnosis of non-melanoma skin cancer

Narasimhan Rajaram, PhD,
Department of Biomedical Engineering, The University of Texas at Austin, Austin, TX 78712

Jason S. Reichenberg, MD,
Department of Dermatology, University of Texas Medical Branch, Austin, TX 78701

Michael R. Migden, MD,
Departments of Dermatology and Plastic Surgery, The University of Texas MD Anderson Cancer Center, Houston, TX 77030

Tri H. Nguyen, MD, and
Mohs & Dermatology Associates, Northwest Diagnostic Clinic PA, Houston, TX 77090

James W. Tunnell, PhD
Department of Biomedical Engineering, The University of Texas at Austin, Austin, TX 78712, 512.232.2110

Narasimhan Rajaram: n.rajaram@mail.utexas.edu; Jason S. Reichenberg: jreichenberg@seton.org; Michael R. Migden: mrmigden@mdanderson.org; Tri H. Nguyen: tnguyenmohs@gmail.com; James W. Tunnell: jtunnell@mail.utexas.edu

Abstract

Background—Several research groups have demonstrated the non-invasive diagnostic potential of diffuse optical spectroscopy (DOS) and laser-induced fluorescence (LIF) techniques for early cancer detection. By combining both modalities, one can simultaneously measure quantitative parameters related to the morphology, function and biochemical composition of tissue and use them to diagnose malignancy. The objective of this study was to use a quantitative reflectance/fluorescence spectroscopic technique to determine the optical properties of normal skin and non-melanoma skin cancers and the ability to accurately classify them. An additional goal was to determine the ability of the technique to differentiate non-melanoma skin cancers from normal skin.

Study Design—The study comprised 48 lesions measured from 40 patients scheduled for a biopsy of suspected non-melanoma skin cancers. White light reflectance and laser-induced fluorescence spectra (wavelength range = 350–700 nm) were collected from each suspected lesion and adjacent clinically normal skin using a custom-built, optical fiber-based clinical instrument. After measurement, the skin sites were biopsied and categorized according to histopathology. Using a quantitative model, we extracted various optical parameters from the measured spectra that could be correlated to the physiological state of tissue.

Results—Scattering from cancerous lesions was significantly lower than normal skin for every lesion group, whereas absorption parameters were significantly higher. Using numerical cut-offs for our optical parameters, our clinical instrument could classify basal cell carcinomas with a

Correspondence to: James W. Tunnell, jtunnell@mail.utexas.edu.

Conflict of Interest: Narasimhan Rajaram and James W. Tunnell receive royalties from the University of Texas through a license agreement with DermDx Inc.

sensitivity and specificity of 94 and 89%, respectively. Similarly, the instrument classified actinic keratoses and squamous cell carcinomas with a sensitivity of 100% and specificity of 50%.

Conclusion—The measured optical properties and fluorophore contributions of normal skin and non-melanoma skin cancers are significantly different from each other and correlate well with tissue pathology. A diagnostic algorithm that combines these extracted properties holds promise for the potential non-invasive diagnosis of skin cancer.

Keywords

Optical spectroscopy; optical properties; non-invasive diagnosis

INTRODUCTION

Skin cancer is the most common form of malignancy with over 2 million new cases of non-melanoma skin cancer (NMSC) expected to be diagnosed in the United States in 2010 [1]. The current procedure for the detection of skin cancers is a clinical examination followed by a tissue biopsy and histopathology – the current gold standard – to confirm the diagnosis. Typically, the number of biopsies performed is at least 5 times the number of new cases of non-melanoma skin cancer detected every year and depends on the experience of the physician. Studies on melanoma skin cancers have shown that general practitioners have a diagnostic accuracy of approximately 40% [2] compared with ~60% for clinically unaided experienced dermatologists [3]. Biopsies are also invasive and time-consuming, requiring on average, a week for patients to receive the results. A real-time, non-invasive and objective method could aid physicians in accurately identifying cancerous lesions and prevent the over-biopsy of benign lesions.

Optical techniques such as diffuse optical spectroscopy and laser-induced fluorescence spectroscopy offer a non-invasive alternative to tissue biopsies for determining the state of tissue. Non-ionizing radiation is delivered and collected with optical fibers that are placed in contact with the skin surface. The weak light pulses sample the tissue beneath the probe non-invasively and are remitted back to the surface where they are collected by fibers located a fixed distance away from the source fiber, providing valuable information regarding the optical scattering, absorption and fluorescence properties of sampled tissue. Physiologically, these properties offer the means to understand the morphology, function and biochemical composition of tissue. Since these physiological parameters of skin change with the progression of disease, optical spectroscopy offers a means to non-invasively measure disease progression in real time. In addition, quantitative optical spectroscopy techniques offer an objective method for diagnosing lesions and do not rely on the experience of the operator.

Diffusely reflected light is a function of the scattering and absorption properties of tissue and hence can provide valuable information regarding tissue morphology and function. Scattering is caused by cells occupying the epidermis as well as collagen present in the dermis. Tissue absorption in the visible spectrum of light is primarily due to hemoglobin in blood vessels and melanin (in case of skin). It is well known that changes in cellular structure and organization in the epidermis, changes in the extra-cellular matrix and angiogenesis are important hallmarks of progression from normal skin to cancer. Researchers have used diffuse reflectance spectroscopy (DRS) to optically visualize these changes and diagnose melanoma [4–7] and non-melanoma skin cancers [8].

Laser-induced fluorescence spectroscopy (LIFS) seeks to exploit biochemical information provided by prominent tissue fluorophores such as collagen, nicotinamide adenine dinucleotide (NADH) and flavin adenine dinucleotide (FAD). NADH and FAD are

important indicators of cellular metabolism. Hence, large-scale cell proliferation or tumor growth can be identified by significant changes in NADH and FAD fluorescence [9]. In addition, studies have reported an increase in production of matrix metalloproteinases (MMPs) with progression to dysplasia [10]. MMPs are a group of collagenases that cleave the collagen crosslinks, which leads to a reduction in the levels of collagen fluorescence. *Ex vivo* studies on non-melanoma skin cancers have confirmed that collagen fluorescence is lower in tumors as compared to normal skin [11]. Panjehpour *et al*. used laser-induced fluorescence to diagnose non-melanoma skin cancers with an accuracy of 93% [12]. However, their accuracy was strongly dependent on the skin type of the patient.

Although DRS and LIFS are independently capable of measuring tissue pathology, a combination of both techniques can provide complementary information about tissue morphology, function and biochemical composition. In addition, acquiring DRS in combination with LIFS allows for correcting the fluorescence spectra distorted by absorption and scattering events [13,14]. Ramanujam and collaborators have conducted extensive studies on malignant breast tissue using a combination of DRS and intrinsic fluorescence (corrected LIFS) spectroscopy (IFS) [15–17]. Clinical studies in the cervix [18] and oral cavity [19] using combined DRS, IFS and model-based light scattering spectroscopy (LSS) have demonstrated that a multimodal approach provides a superior tool for differentiating between normal and dysplastic tissue than any one method alone. A combination of DRS and IFS has been used for *in vivo* cancer diagnosis in the breast with improved results [20].

Several skin imaging devices currently being developed are based on confocal microscopy [21] or optical coherence tomography [22], which provide an *in vivo* image similar to that of histopathology; however, these techniques still requires a trained professional to view and analyze the image. Other proposed systems take multiple photographs of the lesion and use pattern analysis (of size, asymmetry, etc) to predict the malignant potential [23]. The advantage of a spectroscopic device lies in its binary diagnosis (cancer/no cancer) making it an attractive screening tool that can be operated with minimal additional training. It can also ‘look deeper’ into a lesion, relying not just on architecture but also on metabolic composition to make up a diagnosis.

The objective of this study was to determine the optical parameters associated with normal skin and non-melanoma skin cancers, from the measured diffuse reflectance and laser-induced fluorescence spectra. A quantitative analysis of measured spectra has the advantage of providing numerical values and trends that can be correlated to tissue pathology. An additional goal was to determine the ability of a combined quantitative diffuse reflectance/laser-induced fluorescence approach to accurately identify non-melanoma skin cancers. Research studies in the past have utilized only one optical modality – DRS, LIFS or Raman spectroscopy [24–26], for non-invasively identifying skin cancers. However, a combination of two or more optical modalities can provide complementary information regarding tissue architecture and composition, leading to an improvement in diagnostic accuracy [20].

METHODS

Patient recruitment

The study was conducted at the University of Texas Medical Branch, Austin (UTMB) and the Mohs surgery clinic at the M. D. Anderson Cancer Center, Houston (MDACC). The Institutional Review Boards at both institutions approved the study protocol. Informed consent was obtained from all patients who agreed to participate in the study. The participating dermatologist performed a skin examination of the patient and identified suspicious lesions that required a biopsy. We then recorded white light reflectance and laser-

induced fluorescence from each lesion site using our clinical system. The probe tip was placed in gentle contact with the surface of the lesion. Multiple spectra were collected from each site by moving the probe to different locations to sample as much of the lesion as possible. For every lesion site, we also recorded a normal measurement on skin adjacent to the lesion. These normal measurements were made at least 1 cm outside the boundary delineating the lesion. The normal skin was not biopsied. Following spectral measurements, the lesions were biopsied for histological evaluation. For this pilot study, we obtained general biopsy results from the pathologist for the entire lesion and not for specific sampled sites. During classification, the pathology result for the entire site was applied to each spectrum measured from the site.

Clinical instrument

We have developed a fiber optic probe-based clinical instrument that collects both diffuse reflectance and laser-induced fluorescence from skin in less than a second [27]. Briefly, the principal components of the system are: 1) a pulsed xenon flash lamp (Hamamatsu Photonics, Bridgewater, NJ) for white light illumination; 2) a pulsed nitrogen laser (Stanford Research Systems, Mountain View, CA) at 337 nm to excite NADH and collagen fluorescence; 3) a nitrogen-pumped dye laser at 445 nm to excite FAD fluorescence; 4) a MEMS-based fiber optic switch that helps control the excitation sequence of light sources; 5) a bifurcated fiber optic probe for shining and collecting light and 6) an imaging spectrograph (Princeton Instruments, Trenton, NJ) that disperses the collected light onto a 12-bit cooled interline CCD (Roper Scientific, Tucson, AZ) to record spectral data in the wavelength range of 350–700 nm. The system was built on an optical breadboard and mounted on a portable rack (2’ × 2’ × 3’). The portable rack holds the entire optical instrument, the power supply modules and a computer. Additionally, the system contains an uninterruptible power supply (UPS) module on board (run time: 15 minutes) that allows the system to run free of any wall socket and thus allows for its transport between exam rooms. Figure 1 shows an image of the portable clinical system.

The clinical system uses a fiber optic probe to shine and collect light from tissue. The probe head has a diameter of 6.5 mm. The probe consists of 7 optical fibers (diameter = 200 μm; NA = 0.22) arranged in a 6-around-1 configuration with the central fiber illuminating the skin and the six surrounding fibers collecting the diffusely reflected light. The detector fibers are equidistant from the source fiber with a center-center source-detector separation of approximately 250 μm. The size of the probe makes it easy to handle and use on lesions located on the ear and nose. An image of our clinical probe is shown in figure 1. The optical fibers are located at the center of the metal ferrule. The total acquisition time for three sets of white light reflectance and laser-induced fluorescence is typically less than a second. The short exposure time (50 μs) of the camera allows us to collect data with the room lights on, making the system clinically compatible. The spectral measurements from each patient are calibrated against reference standards to enable direct comparison of measured spectra collected on different days.

The spectral diagnosis system has been approved as a Class I laser device by the Laser Safety Board at UT, Austin in accordance with the safety standards specified by the American National Standards Institute (ANSI) [28]. A Class I specification implies the lowest possible risk to skin due to laser exposure, similar to a handheld laser pointer. Care is taken to ensure that the stipulated Class I energy levels are not exceeded during studies on patients.

In vivo data acquisition

Figure 1 presents a detailed flowchart of data acquisition and processing steps using the clinical system. We employ a model-based quantitative analysis of the spectrally resolved diffuse reflectance spectra, R(λ), to determine wavelength-dependent scattering, $\mu_s'(\lambda)$, and absorption properties, $\mu_a(\lambda)$, of sampled tissue. We use the diffuse reflectance spectra in conjunction with the laser-induced fluorescence spectra, F(λ), to extract the native fluorophore contributions of NADH and collagen. The following sections briefly describe the extraction of physiological parameters from diffuse reflectance and intrinsic fluorescence spectra.

Determining optical properties and fluorophore contributions

We recently developed a lookup table (LUT)-based inverse model that can measure tissue optical properties over a physiologically relevant range with an error of less than 10% [29]. The LUT is a database of experimental measurements on calibration standards of known optical properties and is specific to our probe geometry. By constraining the wavelength-dependent scattering and absorption coefficients, we can fit the diffuse reflectance spectra to the LUT and recover valuable physiological information regarding the sampled tissue such as scatter density and size, hemoglobin packaging, blood volume fraction ([Hb]), oxygen saturation (O_2) and melanin concentration ([mel]). To quantify the level of scattering present in the sampled tissue, we measured the reduced scattering coefficient at 630 nm (henceforth referred to as scattering coefficient). We constrained the reduced scattering coefficient to the form,

$$\mu_s'(\lambda)=\mu_s'(\lambda_0)\times\left(\frac{\lambda}{\lambda_0}\right)^{-B}\quad[\mathrm{mm}^{-1}] \tag{1}$$

where λ_0 = 630 nm. Researchers have shown that a power law dependence on wavelength is an appropriate approximation of scattering in bulk tissue [30]. $\mu_s'(\lambda_0)$ and B are indicators of scattering magnitude and scatterer size, respectively. For a homogenous distribution of absorber, the absorption coefficient can be computed as a product of the extinction coefficient and concentration of the absorber. We assumed the absorption in this wavelength range (350–700 nm) to be due to melanin, oxy- and deoxy-hemoglobin. Therefore, we modeled the absorption coefficient as a linear combination of melanin and hemoglobin absorption coefficients, respectively:

$$\mu_{a(tissue)}(\lambda)=[\mathrm{mel}]\times\varepsilon_{\mathrm{mel}}(\lambda)+[\mathrm{Hb}]\times[\alpha\varepsilon_{\mathrm{HbO}_2}(\lambda)+(1-\alpha)\varepsilon_{\mathrm{Hb}}(\lambda)]\quad[\mathrm{mm}^{-1}] \tag{2}$$

where [mel] and [Hb] represent the concentrations of melanin and hemoglobin, respectively. α is the oxygen saturation representing the ratio of oxygenated to total hemoglobin concentration and $\varepsilon_{\mathrm{mel}}(\lambda)$, $\varepsilon_{\mathrm{HbO2}}(\lambda)$ and $\varepsilon_{\mathrm{Hb}}(\lambda)$ are the extinction coefficients of melanin, oxygenated and deoxygenated hemoglobin, respectively. However, these equations are only valid for a homogeneous distribution of absorber. Because hemoglobin is confined to very small volumes such as blood vessels, we have to account for this inhomogeneous distribution in tissue. We use the correction equations described by van Veen [31] to calculate a corrected absorption coefficient of blood. The correction factor can be calculated as,

$$C_{pack}=\left\lfloor \frac{1-\exp(-2\mu_{a,bl}(\lambda)r_{vess})}{2\mu_{a,bl}(\lambda)r_{vess}} \right\rfloor \quad [3]$$

where $\mu_{a,bl}(\lambda)$ is the absorption coefficient of whole blood and r_{vess} is assumed to be the mean vessel radius in the tissue volume sampled. We assume the hemoglobin concentration in whole blood to be 150 mg/ml and calculate the absorption coefficient of whole blood as:

$$\mu_{a,bl}(\lambda)=150\times[\alpha\varepsilon_{HbO_2}(\lambda)+(1-\alpha)\varepsilon_{Hb}(\lambda)] \quad [\mathrm{mm}^{-1}] \quad [4]$$

The packaging corrected absorption coefficient of blood in tissue can now be written as:

$$\mu_{a(Hb)}^{corrected}(\lambda)=C_{pack}\nu\mu_{a,bl}(\lambda) \quad [\mathrm{mm}^{-1}], \quad [5]$$

where ν denotes the blood volume fraction sampled by the light assuming a hemoglobin concentration of 150 mg/ml. The blood volume fraction can also be expressed as [Hb]/150. Thus, the blood volume fraction is a measure of the effective or volume-averaged hemoglobin concentration that is sampled by the light, assuming the whole blood hemoglobin concentration in the blood vessels is 150 mg/ml. The correction factor described above and subsequent equations used to model an inhomogeneous distribution in tissue have been validated in blood-vessel like microfluidic devices in a recent publication by our group [32].

We used the model described by Zhang *et al.* [13] to extract the intrinsic fluorescence of a fluorophore by combining the diffuse reflectance and laser-induced fluorescence spectra. The intrinsic fluorescence due to 337 nm excitation consists of two dominant fluorophores, NADH with a peak at 450 nm and collagen with a fluorescence peak at 410 nm [33]. Depending on the relative contributions of NADH and collagen, the intrinsic fluorescence spectrum is either red-shifted toward 450 nm or blue-shifted toward 410 nm. We determined the individual contributions of these fluorophores from the intrinsic fluorescence spectrum using a linear combination of their basis spectra and a least-squares fitting routine. The intrinsic fluorescence due to 445 nm excitation was considered to be only due to FAD and is not discussed in this paper. The basis spectra for NADH and collagen used in this paper were adapted from previous work done in the esophagus [34].

Statistical analysis

It is well known that the physiology of skin varies across the body. These physiological differences can lead to wide changes in the optical properties of normal skin. Hence, it may be difficult or even impossible to compare lesions at different anatomical locations without standardization. Therefore, we determined the diagnostic potential of our system after standardization of the data. To perform the standardization, we calculated a mean reflectance and fluorescence value for normal skin, based on all measured normal skin sites on all patients and standardized all normal measurements to this value. Similarly, all lesion spectra were normalized to their respective normal sites and standardized to the baseline reflectance/fluorescence value. When multiple normal measurements existed for a lesion site, we normalized all lesion spectra to the peak (*max*) reflectance or fluorescence of the first normal spectrum [$N_1(\lambda)$] measured. The peak value is the highest reflectance or fluorescence measured across a single spectrum. The process can be summarized by the following equations:

$$N_i(\lambda)=\frac{N_i(\lambda)}{\max[N_1(\lambda)]}\times N_{mean} \quad [6]$$

$$L_i(\lambda)=\frac{L_i(\lambda)}{\max[N_1(\lambda)]}\times N_{mean}, \quad [7]$$

where $N_i(\lambda)$ and $L_i(\lambda)$ represents wavelength-dependent reflectance or fluorescence spectra from normal skin and lesions, respectively. Here, *i* denotes spectra measured from each lesion. The second term in both equations (N_{mean}) represents calculation of the mean reflectance or fluorescence value for all normal skin sites collected in this study. The result of such standardization is that normal spectra are scaled up or down to center around this mean value; the lesion spectra are now normalized to their respective normal spectra. This retains the original differences between normal and lesion while removing large variations in normal skin due to anatomical site. The only change to the spectra is in terms of magnitude; the shape of the reflectance and fluorescence spectra remains the same. We extracted the physiological parameters of the standardized spectra and determined the diagnostic accuracy of the system for each cancer group based on these physiological parameters. Although we standardize the data for comparing normal skin and lesions, we used the absolute values for reporting the absolute optical properties and physiological parameters and standardized data for determining the diagnostic potential of DRS-IFS.

For both methods, our statistical analysis of the data consisted of two steps. First, we used one-way analysis of variance (ANOVA) to determine the physiological parameters that showed statistically significant differences between each cancerous group and its corresponding normal skin site. Classification of each site was based on the results of histopathology. Second, we used logistic regression and leave-one-out cross validation [35] to determine the diagnostic potential of a combination of physiological parameters in classifying normal from cancerous skin. We calculated the area under the receiver operating curve (ROC) for different combinations of physiological parameters and selected the combination with the highest area for spectral diagnosis. Because we made multiple spectral measurements on each lesion and corresponding normal skin, our spectral diagnosis for lesions and normal skin sites was as follows: If 1 or more spectra from a site were classified as cancer, the site was classified as a cancer. If all spectra from a site were classified as normal, the site was assigned to the normal group. The basis for such classification was the dermatologist's approach to err on the side of caution. Since AK is considered a precursor to SCC, we conducted the classification for AK and SCC in a stepwise manner. Using our diagnostic algorithm, we first separated the normals from AKs and SCCs. All measurements that were correctly identified as cancer (AK or SCC) were further separated into two groups: AK or SCC. In the results section, we report the number of correctly classified spectra as well as lesions. The accuracy based on lesions was calculated using the procedure mentioned above.

RESULTS

Overall, we measured 147 (91 lesion and 56 normal) sets of reflectance and fluorescence spectra from patients with suspected lesions. This corresponds to 48 suspected lesions on 40 different patients, with a few patients having multiple suspicious lesions. Table 1 summarizes the total number of spectra, skin sites and patients included in the study. The average size of the lesions measured in the study was approximately 7 mm. This is very

close to the diameter of the probe head. Therefore, we did not encounter problems with probe placement on lesions. Table 2 documents the anatomical location of the lesions included in this study.

Figure 2 shows representative diffuse reflectance and intrinsic fluorescence spectra (337 nm excitation) from each cancerous group (BCC, AK and SCC) and their respective normal skin sites. These represent calibrated *in vivo* measurements and are not standardized spectra. The shape of the diffuse reflectance spectrum is derived from the natural negative slope of scattering in tissue and the typical oxy-hemoglobin absorption peaks at 420, 542 and 577 nm. The circles indicate the LUT model fit to the data, demonstrating excellent agreement between the measured *in vivo* reflectance and the LUT model.

The overall diffuse reflectance intensity across all wavelengths was found to be consistently lower for cancerous groups when compared to the respective normal spectra. Data analysis of the diffuse reflectance spectra revealed statistically significant differences ($p < 0.05$) in the optical properties between normal skin and the different histologic groups. This data is represented in the form of bar plots in Figure 3. The blood vessel diameter and the blood volume fraction were significantly larger in malignant BCC compared to the respective normal skin sites. This is evidenced by the line shape of the diffuse reflectance spectra of BCC, which show large depressions in the Soret (420 nm) and Q-bands (540–575 nm) of hemoglobin absorption. Similar trends were also noticed for AK and SCC; however, these were not found to be statistically significant. The scattering coefficient was significantly lower for every cancerous group when compared to normal skin. All the patients enrolled in the study were Caucasian (Skin Type I or II). Even though we incorporated melanin in our model (eumelanin from Steve Jacques's compilation [36]), there was little to no contribution from melanin. Therefore, we do not present a discussion of melanin here.

Figure 4 shows the extracted contributions of NADH and collagen to 337 nm-excited intrinsic fluorescence. Although not statistically significant, the collagen levels decreased with progression from normal skin to BCC. However, the collagen level increased in the case of progression from normal skin to AK and SCC. We did not observe any statistically significant trends with NADH fluorescence.

Figure 5 shows scatter plots of physiological parameters used to discriminate each cancerous group from normal skin. The solid line is the decision line separating the two groups. Figure 5a clearly demonstrates that BCC lesions have a significantly lower scattering coefficient and a higher mean vessel diameter. A similar trend can be noted for separating normal sites from AK and SCC lesions [Fig. 5b]. The most significant physiological parameters for classifying AK and SCC were found to be collagen and oxygen saturation, with both being significantly lower for the SCC lesions. Based on our analysis of the BCC group, we could correctly classify 36/39 BCC and 21/23 normal spectra. For the AK/SCC group, we first separated the normal spectra ($n = 33$) from all AK and SCC spectra combined ($n = 52$). We were able to correctly classify 47/52 lesion spectra and 20/33 normal spectra. We then used the algorithm to separate AKs from SCCs. The algorithm correctly classified 26/34 SCC and 8/18 AK spectra.

To better compare our results to dermatologists' performance, we calculated the sensitivity and specificity of our instrument based on the lesions. By this metric, the algorithm correctly classified 17/18 BCC lesions and 16/18 corresponding normal skin measurements. This corresponds to a sensitivity and specificity of 94 and 89%, respectively. Similarly, following a two-step classification process, the diagnostic algorithm correctly classified 18/18 SCC lesions and 6/12 AKs. This corresponds to a sensitivity of 100% and a specificity of 50%.

Table 3 presents a detailed comparison of the sensitivity and specificity values for DRS, IFS and combined DRS-IFS for each cancer group.

Table 4 presents a comparison of both spectral and clinical diagnosis (dermatologist) to pathology for classifying AK and SCC lesions. Both clinical and spectral diagnoses achieved 100% sensitivity for diagnosing SCC lesions. However, the specificity of spectral diagnosis was 50%-over 6 times higher than the dermatologists, who achieved a specificity of 8.3%.

DISCUSSION

This paper describes a quantitative optical spectroscopy system for the purpose of differentiating normal skin and non-melanoma skin cancers. The clinical system performs an 'optical biopsy' of the cancerous lesion within a fraction of a second, measuring both diffuse reflectance and fluorescence spectra. We use a lookup table-based model to measure the optical properties and physiological parameters of sampled skin on a small population of subjects with non-melanoma skin cancers. Our results compare well with previously published studies [8,25,37]. In contrast to these reports, our study is based on a quantitative analysis of the spectra in the form of physiological parameters. Using a quantitative approach to diagnosing lesions has a number of advantages. First, it provides us with numerical values and trends that can be understood in the physiological context correlated with pathology. Second, it provides an objective method for classifying lesions independent of physician or pathologist experience. Third, as a diagnostic aid, it does not require learning on the part of the physician to interpret the results. This pilot clinical study demonstrates that optical spectroscopy measures significant changes associated with tissue pathology, and when used diagnostically, optical spectroscopy may hold promise as a non-invasive diagnostic aid for skin cancer. We are currently planning a larger clinical trial where we hope to use the diagnostic information acquired from this study to diagnose lesions in the clinic.

The data analysis revealed statistically significant differences in optical properties between normal skin and NMSC. Normal skin was shown to have the highest magnitude of diffuse reflectance from skin across all three groups of lesions. There is a decrease in the overall intensity of the DRS spectra with progression to pre-cancerous AK and SCC and BCC. This was further validated by statistically significant changes in scattering coefficient ($p < 0.001$), which represents the magnitude of scattering from tissue. These changes can be attributed to at least two mechanisms. First, there could be a breakdown in the collagen matrix present in the dermis. The contribution of collagen to the overall scattering at the source-detector separation exceeds that of cells and nuclei. Because of this, a small increase in the epidermal scattering due to large-scale malignant cell proliferation would still be masked by a larger reduction in dermal collagen scattering. This trend in scattering from normal to malignant cancer is consistent with previous studies on skin [8,38]. Second, our instrument uses a fiber optic probe configuration to shine and collect light from superficial tissue layers. We estimate the sampling depth of the probe to be ~250–300 μm. An increase in the thickness of the epidermis with progression of malignancy could reduce the amount of collagen being sampled by the probe. This could also lead to a decrease in scattering from the malignant groups. Both these hypotheses are supported by Figure 6, which shows micrographs of tissue sections stained with hematoxylin and eosin (top row), and trichrome (bottom row) for collagen. Figure 6a shows normal skin on the left side of the image that gradually progresses to AK on the right. The thickening of the epidermis is very visible in this case. Similarly, Fig. 6e (BCC) demonstrates decreased collagen staining in the dermis, which is consistent with our spectrographic findings when compared to normal skin (Fig. 6d).

However, there is no noticeable increase in epidermal thickness with progression from normal to BCC.

The data also showed differences in the absorption properties of normal skin and malignant lesions. Specifically, we noted a statistically significant increase in mean vessel diameter and blood volume fraction with progression from normal skin to BCC, consistent with similar trends noticed in the oral cavity [39]. These trends are consistent with tumor physiology and behavior. Angiogenesis is a well-established phenomenon and studies have shown that tumors tend to spawn production of a network of blood vessels and exhibit higher absorption [40].

In addition to the optical properties extracted from DRS spectra, we also determined the biochemical composition of tissue from IFS spectra. Our analysis showed that the contribution of collagen decreased with progression from normal skin to malignant BCC. A decrease in collagen signal has also been shown using Raman spectroscopy [25]. This trend is consistent with our explanation for the reduction in scattering due to either destruction of the collagen matrix or a decrease in probe sampling depth. However, this trend does not hold true for the other two groups, as the collagen contribution of AK and malignant SCC are higher than the respective normal groups. Although there is a reduction in collagen concentration in SCC when compared to AK and can be explained with reasons similar to that of scattering, we do not completely understand the reasons for an increase in the fluorescence levels from normal to AK. An almost uniform feature of the measured AKs and SCCs was the crusted appearance of the lesion. Because of the thicker stratum corneum, there could be an increase in the keratin present. This characteristic could have altered the sampling depth of our probe, causing a trend contrary to previously established reports. Keratin fluoresces in the same region as NADH and has two fluorescence excitation peaks at 277 and 297 nm; however, given our excitation wavelength (337 nm), we do not believe that keratin is contributing to the fluorescence signal. Previous studies have reported an increase in production of matrix metalloproteinases (MMPs), a group of collagenases that cleave the collagen crosslinks and lead to a reduction in the level of fluorescence from collagen [10]. Although not statistically significant, we also noticed a slight decrease in NADH contribution. NADH is a by-product of cellular metabolism and one would expect it to increase with large-scale cell proliferation as seen in malignant lesions. However, the contribution of NADH decreased in BCC and SCC as compared to normal skin. This trend is contrary to what has been reported by other researchers [34].

We used a standardization method to remove differences between the normal skin spectra measured on different parts of the body. This procedure helps eliminate false positive results in the clinical analysis. The standardization procedure creates a baseline value for normal skin reflectance and normalizes all the spectra to this value. This has not been fully explored in previous studies of the reflectance or intrinsic florescence of other anatomic sites, possibly due to the more uniform anatomic layer found throughout large areas of the cervix or esophagus. However, a few lesion spectra still get classified as normal skin. This could be attributed to the heterogeneous nature of skin tumors. We hope to use larger-scale studies to further classify the lesions (nodular BCC, superficial BCC, etc) to see if this would account for the differences seen. In addition, because we are making a small and finite number of measurements of a large lesion, it is possible that some of the false negatives could have been measured on areas that did not show signs of dysplasia. We are working on a modification of our device that would take a larger number of automated measurements from each lesion to decrease the possibility of sampling error.

We used only two parameters to classify the lesions in each cancerous group. For BCC lesions, we determined that a combination of mean vessel diameter and scattering coefficient

provided the best classification between normal and cancerous skin. A combination of reflectance and fluorescence parameters was found to provide higher sensitivity and specificity for classifying AKs and SCCs.

The sensitivity and specificity of diagnosing BCC lesions using our algorithm was 94 and 89%, respectively. Although we compare BCCs to normal skin in our study, we eventually hope to expand the study population to include benign lesions such as warts, scars and seborrhoeic keratoses to BCCs. We will follow a two-step strategy similar to the AK/SCC classification to separate normals from benign lesions and BCCs. The clinical distinction of normal skin from BCCs assumes significance in the area of tumor margin demarcation. Although it is possible for dermatologists to be highly accurate in differentiating normal skin from cancers, demarcating the exact tumor margins and thereby reducing recurrence as well as excess removal of normal tissue is a significant problem. Spectral diagnosis using our instrument could act as a diagnostic aid for dermatologists to quantitatively determine the borders of a tumor and help reduce the amount of tissue removed.

Following a two-step diagnostic process, we separated the AK from SCC lesions with a sensitivity of 100% and a specificity of 50%. We have not been able to find other studies that exclusively classify AKs and SCCs. Previous clinical studies using DRS or Raman spectroscopy have typically grouped AKs with other benign or pre-cancerous lesions and/or SCCs with other malignant lesions [8,37]. Our specificity represents a significant increase over the dermatologists' performance (8.3%), while providing excellent sensitivity. The sensitivity and specificity of dermatologists reported is specific to this study for the classification of AKs and SCCs. A number of studies that compared the performance of dermatologists with and without visual aids such as dermoscopes have reported sensitivity and specificity values in the range of 60–90% [3]; the better numbers typically correspond to diagnosis of BCCs [41]. In our clinical study, a majority of suspected SCC lesions were clinically diagnosed (by dermatologist) as either AK or SCC. Distinguishing AKs from SCCs has been acknowledged as an important diagnostic problem in dermatology [42,43] because AKs are frequently indistinguishable from SCCs without a biopsy [44]. We believe that the specificity demonstrated by our instrument, although higher than the dermatologist, can be further improved by modifying the clinical probe. The clinical probe has a fixed fiber optic source-detector separation that probes a specific depth in tissue. A progression of AKs to SCCs would be noticed in terms of depth; AKs are typically restricted to the deeper layers of epidermis while SCCs are present in the entire epidermis and progressively invade the dermis and lymph nodes [45]. A multi-separation probe consisting of different source-detector separations that samples different depths in tissue could potentially identify such a progression. Such a probe has been investigated previously for diagnosis of breast cancer [46]. Our current sensitivity and superior specificity holds promise for future large-scale clinical trials.

Based on our results, spectral diagnosis could have potentially saved 42% of the extra biopsies performed. Table 6 shows that the over-biopsy rate in the clinics where the study was conducted was approximately 67% (12/18). Considering this over-biopsy rate and the fact that approximately 300,000 SCCs are diagnosed every year in the United States, our instrument could have avoided 84,000 skin biopsies. To put this in a much larger perspective, the American Cancer Society (ACS), predicts that over 2 million non-melanoma skin cancers will be diagnosed in 2010 [1]. Assuming that at least 4 biopsies are performed before a skin cancer is caught, 42% of 8 million extra biopsies could be avoided, saving patients well over a billion dollars, in addition to the morbidity associated with such procedures. This is a very conservative estimate and presents a brief insight into the amount of money and time that could be saved by potentially using this instrument as a non-invasive diagnostic aid for dermatologists. Additionally, a shortage of experienced dermatologists

means that the burden of early detection of important skin cancers such as melanomas falls on primary care physicians. Such an instrument would be extremely useful as a screening tool in the hands of primary care physicians who do not perform as well as expert dermatologists [47]. Because lesions can typically be scanned using our instrument in less than a second, the physician can quickly sample several sites on a patient and either immediately rule out cancer or refer suspicious lesions to dermatologists. Therefore, a non-invasive instrument would catch more cancers at an early stage, reduce the number of referrals to dermatologists and finally reduce unnecessary biopsies.

Acknowledgments

We would like to thank Drs. Brent Talbot and Anthony Soldano for providing us with some of the pathology slides. We would also like to thank Olga Heinle, Clinical Research Coordinator for all her support and help throughout the clinical study. We are also indebted to the patients who agreed to participate in this study.

Funding/Support: This study was supported in part by a translational research award from the Wallace H. Coulter Foundation and the National Institutes of Health (Grant No. R01 CA132032).

References

1. Jemal, A.; Siegel, R.; Xu, J.; Ward, E. Cancer statistics. CA: A Cancer Journal for Clinicians; 2010.
2. Moreno G, Tran H, Chia A, Lim A, Shumack S. Prospective study to assess general practitioners' dermatological diagnostic skills in a referral setting. Australasian Journal of Dermatology. 2007; 48(2):77. [PubMed: 17535192]
3. Kittler H, Pehamberger H, Wolff K, Binder M. Diagnostic accuracy of dermoscopy. Lancet Oncol. 2002; 3(3):159–165. [PubMed: 11902502]
4. Marchesini R, Cascinelli N, Brambilla M, Clemente C, Mascheroni L, Pignoli E, Testori A, Venturoli D. *In vivo* spectrophotometric evaluation of neoplastic and non-neoplastic skin pigmented lesions. II: Discriminant analysis between nevus and melanoma. Photochem Photobiol. 1992; 55(4): 515–522. [PubMed: 1620728]
5. Wallace VP, Crawford DC, Mortimer PS, Ott RJ, Bamber JC. Spectrophotometric assessment of pigmented skin lesions: methods and feature selection for evaluation of diagnostic performance. Phys Med Biol. 2000; 45(3):735–751. [PubMed: 10730968]
6. Murphy BW, Webster RJ, Turlach BA, Quirk CJ, Clay CD, Heenan PJ, Sampson DD. Toward the discrimination of early melanoma from common and dysplastic nevus using fiber optic diffuse reflectance spectroscopy. J Biomed Opt. 2005; 10(6):064020. [PubMed: 16409085]
7. Zonios G, Dimou A, Bassukas I, Galaris D, Tsolakidis A, Kaxiras E. Melanin absorption spectroscopy: new method for noninvasive skin investigation and melanoma detection. J Biomed Opt. 2008; 13(1):014017. [PubMed: 18315375]
8. Garcia-Uribe A, Kehtarnavaz N, Marquez G, Prieto V, Duvic M, Wang LV. Skin cancer detection by spectroscopic oblique-incidence reflectometry: classification and physiological origins. Appl Opt. 2004; 43(13):2643–2650. [PubMed: 15130003]
9. Skala MC, Riching KM, Gendron-Fitzpatrick A, Eickhoff J, Eliceiri KW, White JG, Ramanujam N. In vivo multiphoton microscopy of NADH and FAD redox states, fluorescence lifetimes, and cellular morphology in precancerous epithelia. PNAS. 2007; 104(49):19494–19499. [PubMed: 18042710]
10. Drezek R, Brookner C, Pavlova I, Boiko I, Malpica A, Lotan R, Follen M, Richards-Kortum R. Autofluorescence microscopy of fresh cervical-tissue sections reveals alterations in tissue biochemistry with dysplasia. Photochem Photobiol. 2001; 73(6):636–641. [PubMed: 11421069]
11. Brancaleon L, Durkin AJ, Tu JH, Menaker G, Fallon JD, Kollias N. *In vivo* fluorescence spectroscopy of nonmelanoma skin cancer. Photochem Photobiol. 2001; 73(2):178–183. [PubMed: 11272732]
12. Panjehpour M, Julius CE, Phan MN, Vo-Dinh T, Overholt S. Laser-induced fluorescence spectroscopy for in vivo diagnosis of non-melanoma skin cancers. Lasers Surg Med. 2002; 31(5): 367–373. [PubMed: 12430156]

13. Zhang Q, Muller MG, Wu J, Feld MS. Turbidity-free fluorescence spectroscopy of biological tissue. Opt Lett. 2000; 25(19):1451–1453. [PubMed: 18066245]
14. Palmer GM, Ramanujam N. Monte-Carlo-based model for the extraction of intrinsic fluorescence from turbid media. J Biomed Opt. 2008; 13(2):024017. [PubMed: 18465980]
15. Zhu C, Palmer GM, Breslin TM, Harter J, Ramanujam N. Diagnosis of breast cancer using fluorescence and diffuse reflectance spectroscopy: a Monte-Carlo-model-based approach. J Biomed Opt. 2008; 13(3):034015. [PubMed: 18601560]
16. Zhu C, Breslin TM, Harter J, Ramanujam N. Model based and empirical spectral analysis for the diagnosis of breast cancer. Opt Exp. 2008; 16(19):14961–14978.
17. Palmer GM, Zhu C, Breslin TM, Xu F, Gilchrist KW, Ramanujam N. Comparison of multiexcitation fluorescence and diffuse reflectance spectroscopy for the diagnosis of breast cancer (March 2003). IEEE Trans Biomed Eng. 2003; 50(11):1233–1242. [PubMed: 14619993]
18. Georgakoudi I, Sheets EE, Muller MG, Backman V, Crum CP, Badizadegan K, Dasari RR, Feld MS. Trimodal spectroscopy for the detection and characterization of cervical precancers *in vivo*. Am J Obstet Gynecol. 2002; 186(3):374–382. [PubMed: 11904594]
19. Muller M, Valdez T, Georgakoudi I, Backman V, Fuentes C, Kabani S, Laver N, Wang Z, Boone C, Dasari R. Spectroscopic detection and evaluation of morphologic and biochemical changes in early human oral carcinoma. Cancer. 2003; 97(7):1681–1692. [PubMed: 12655525]
20. Volynskaya Z, Haka AS, Bechtel KL, Fitzmaurice M, Shenk R, Wang N, Nazemi J, Dasari RR, Feld MS. Diagnosing breast cancer using diffuse reflectance spectroscopy and intrinsic fluorescence spectroscopy. J Biomed Opt. 2008; 13(2):024012. [PubMed: 18465975]
21. Patel Y, Nehal K, Aranda I, Li Y, Halpern A, Rajadhyaksha M. Confocal reflectance mosaicing of basal cell carcinomas in Mohs surgical skin excisions. J Biomed Opt. 2007; 12:034027. [PubMed: 17614735]
22. Jorgensen T, Tycho A, Mogensen M, Bjerring P, Jemec G. Machine-learning classification of non-melanoma skin cancers from image features obtained by optical coherence tomography. Skin Research and Technology. 2008; 14(3):364–369. [PubMed: 19159385]
23. Gutkowicz-Krusin D, Elbaum M, Jacobs A, Keem S, Kopf A, Kamino H, Wang S, Rubin P, Rabinovitz H, Oliviero M. Precision of automatic measurements of pigmented skin lesion parameters with a MelaFindTM multispectral digital dermoscope. Melanoma Research. 2000; 10(6):563. [PubMed: 11198478]
24. Gniadecka M, Wulf H, Nymark Mortensen N, Faurskov Nielsen O, Christensen D. Diagnosis of basal cell carcinoma by Raman spectroscopy. Journal of Raman Spectroscopy. 1997; 28(23):125–129.
25. Nijssen A, Maquelin K, Santos L, Caspers P, Schut T, den Hollander J, Neumann M, Puppels G. Discriminating basal cell carcinoma from perilesional skin using high wave-number Raman spectroscopy. J Biomed Opt. 2007; 12:034004. [PubMed: 17614712]
26. Lieber C, Majumder S, Billheimer D, Ellis D, Mahadevan-Jansen A. Raman microspectroscopy for skin cancer detection in vitro. J Biomed Opt. 2008; 13:024013. [PubMed: 18465976]
27. Rajaram N, Aramil TJ, Lee K, Reichenberg JS, Nguyen TH, Tunnell JW. Design and validation of a clinical instrument for spectral diagnosis of cutaneous malignancy. Appl Opt. 2010; 49(2):142–152. [PubMed: 20062500]
28. American National Standard for safe use of lasers. American National Standard Institute; Z1361-2000
29. Rajaram N, Nguyen TH, Tunnell JW. Lookup table-based inverse model for determining optical properties of turbid media. J Biomed Opt. 2008; 13(5):050501. [PubMed: 19021373]
30. Mourant JR, Fuselier T, Boyer J, Johnson TM, Bigio IJ. Predictions and measurements of scattering and absorption over broad wavelength ranges in tissue phantoms. Appl Opt. 1997; 36(4):949–957. [PubMed: 18250760]
31. van Veen RL, Verkruysse W, Sterenborg HJ. Diffuse-reflectance spectroscopy from 500 to 1060 nm by correction for inhomogeneously distributed absorbers. Opt Lett. 2002; 27(4):246–248. [PubMed: 18007768]

32. Rajaram N, Gopal A, Zhang X, Tunnell JW. Experimental validation of the effects of microvasculature pigment packaging on in vivo diffuse reflectance spectroscopy. Lasers Surg Med. 2010; 42(7):680–688. [PubMed: 20740619]
33. Ramanujam N. Fluorescence spectroscopy of neoplastic and non-neoplastic tissues. Neoplasia. 2000; 2(1–2):89–117. [PubMed: 10933071]
34. Georgakoudi I, Jacobson BC, Muller MG, Sheets EE, Badizadegan K, Carr-Locke DL, Crum CP, Boone CW, Dasari RR, Van Dam J, Feld MS. NAD(P)H and collagen as *in vivo* quantitative fluorescent biomarkers of epithelial precancerous changes. Cancer Research. 2002; 62(3):682–687. [PubMed: 11830520]
35. Schumacher M, Hollander N, Sauerbrei W. Resampling and cross-validation techniques: a tool to reduce bias caused by model building? Statistics in medicine. 1997; 16(24):2813–2827. [PubMed: 9483716]
36. Jacques, S. Optical absorption of melanin. 1998. http://omlc.ogi.edu/spectra/melanin/index.html
37. Lieber C, Majumder S, Ellis D, Billheimer D, Mahadevan-Jansen A. In vivo nonmelanoma skin cancer diagnosis using Raman microspectroscopy. Lasers Surg Med. 2008; 40(7)
38. Salomatina E, Jiang B, Novak J, Yaroslavsky AN. Optical properties of normal and cancerous human skin in the visible and near-infrared spectral range. J Biomed Opt. 2006; 11(6):064026. [PubMed: 17212549]
39. Amelink A, Sterenborg HJ, Bard MP, Burgers SA. *In vivo* measurement of the local optical properties of tissue by use of differential path-length spectroscopy. Opt Lett. 2004; 29(10):1087–1089. [PubMed: 15181994]
40. Folkman J. What is the evidence that tumors are angiogenesis dependent? J Natl Cancer Inst. 1990; 82(1):4–6. [PubMed: 1688381]
41. Brown S, Lawrence C. The management of skin malignancy: to what extent should we rely on clinical diagnosis? British Journal of Dermatology. 2006; 155(1):100–103. [PubMed: 16792759]
42. Lober B, Lober C, Accola J. Actinic keratosis is squamous cell carcinoma. Southern Medical Journal. 2000; 93(7):650–656. [PubMed: 10923948]
43. Salasche S. Epidemiology of actinic keratoses and squamous cell carcinoma. J Am Acad Dermatol. 2000; 42(1):4. [PubMed: 10607349]
44. Moy R. Clinical presentation of actinic keratoses and squamous cell carcinoma. J Am Acad Dermatol. 2000; 42(1):8. [PubMed: 10607350]
45. Anwar J, Wrone DA, Kimyai-Asadi A, Alam M. The development of actinic keratosis into invasive squamous cell carcinoma: Evidence and evolving classification schemes. Clinics in Dermatology. 2004; 22(3):189–196. [PubMed: 15262304]
46. Zhu C, Palmer GM, Breslin TM, Xu F, Ramanujam N. Use of a multiseparation fiber optic probe for the optical diagnosis of breast cancer. J Biomed Opt. 2005; 10(2):024032. [PubMed: 15910105]
47. Chen SC, Pennie ML, Kolm P, Warshaw EM, Weisberg EL, Brown KM, Ming ME, Weintraub WS. Diagnosing and managing cutaneous pigmented lesions: primary care physicians versus dermatologists. J Gen Intern Med. 2006; 21(7):678–682. [PubMed: 16808765]

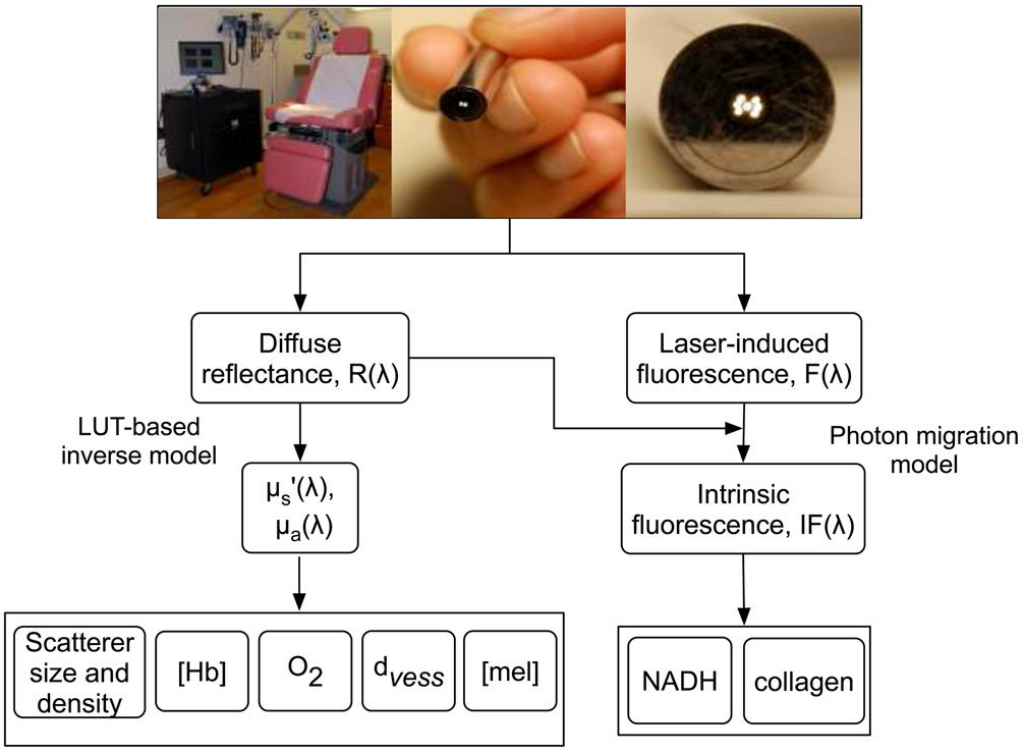

Figure 1.
Flowchart describing data acquisition and processing using the clinical system.

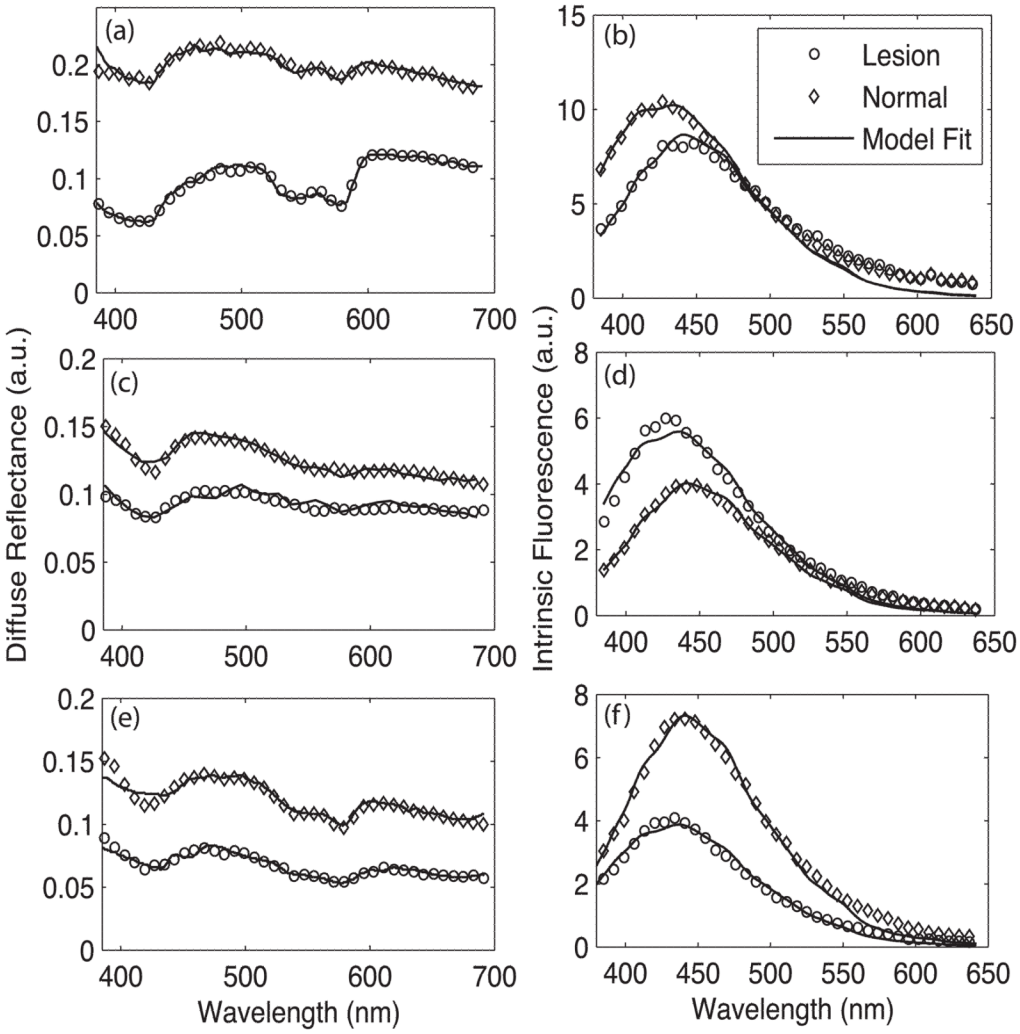

Figure 2.

Representative *in vivo* diffuse reflectance spectra (circles) from (a) malignant BCC, (c) pre-cancerous AK and (e) malignant SCC. The thin lines indicate LUT model fit. Also shown are the normal skin site measurements (diamonds). The corresponding intrinsic fluorescence spectra from 337 nm excitation for each cancerous group are shown in panels (b), (d) and (f).

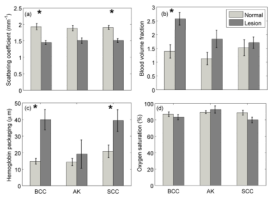

Figure 3.

Mean physiological parameters of NMSC and respective normal skin sites measured using the LUT-based model. The error bars represent standard error. Stars indicate statistically significant differences between normal and cancerous skin.

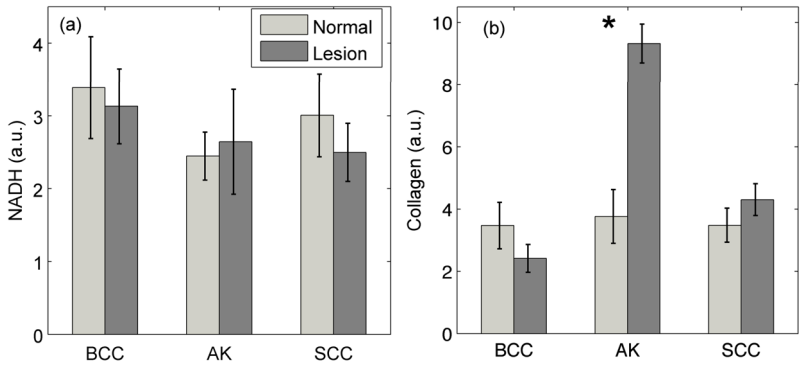

Figure 4.

Mean fluorophore contributions of NMSC and respective normal skin sites measured using the intrinsic fluorescence model and linear combination analysis. The error bars represent standard error.

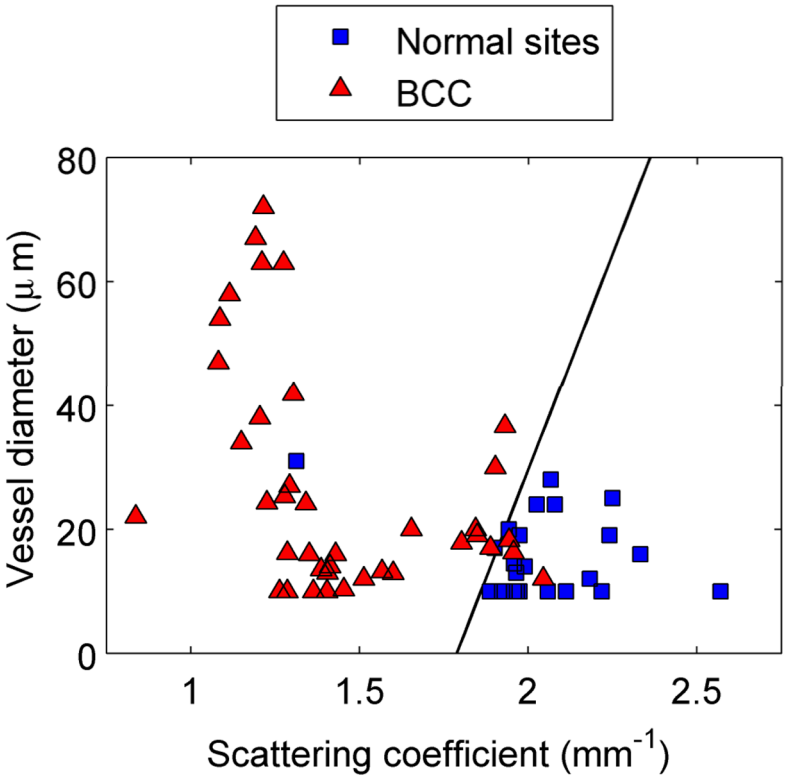

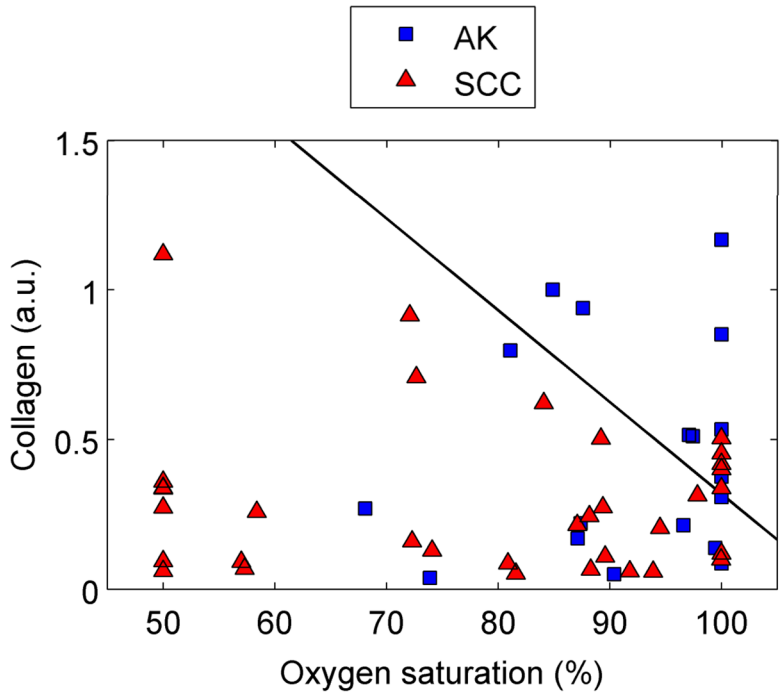

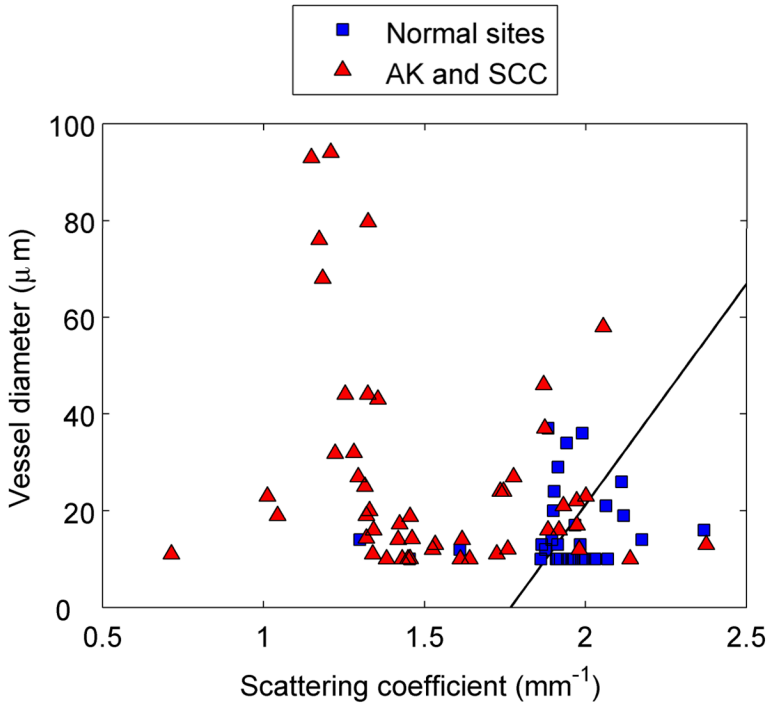

Figure 5.
Discrimination of NMSC using logistic regression and leave-1-out validation. (a) Normal skin from BCC lesions. (b) Normal skin from grouped AKs and SCCs. (c) AKs from SCCs.

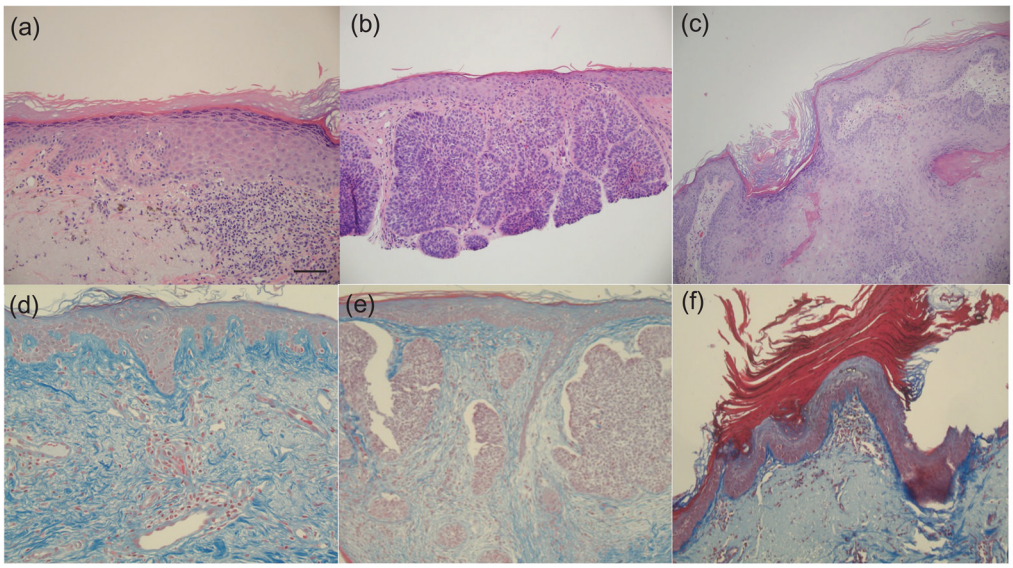

Figure 6.
Micrographs showing hematoxylin and eosin-stained sections (100x) from (a) AK (b) BCC and (c) SCC. The bottom row shows images of trichrome-stained sections of (d) normal skin (20x), (e) BCC (10x) and (f) AK (10x); collagen shows up as a blue color. Note abundant collagen in the normal skin image.

Table 1

Classification of skin lesions included in the study, based on histopathology.

Classification	Patients	Sites	Spectra	
			Normal	Lesion
AK	11	12	14	18
SCC	15	18	19	34
BCC	14	18	23	39
Total	**40**	**48**	**56**	**91**

Table 2

Anatomical location of each site included in the study.

Classification	AK	SCC	BCC
Arm	3	6	2
Face	5	6	12
Head and Neck	2	2	-
Leg	-	2	-
Chest	1	2	3
Back	1	-	1
Total Sites	**12**	**18**	**18**

Table 3

Performance of each optical modality in classifying normal and lesion spectra from the three cancerous groups. These numbers are based on the lesions. The numbers shown in bold represent the best possible diagnosis using parameters shown in Figure 5.

Optical modality	Normal vs. BCC		Normal vs. AK and SCC		AK vs. SCC	
	Sens.	Spec.	Sens.	Spec.	Sens.	Spec.
DRS	**94**	**89**	**97**	**62**	89	25
IFS	83	11	70	18	83	25
DRS + IFS	94	61	90	57	**100**	**50**

Table 4

A comparison of clinical and spectral diagnosis for classifying AK and SCC lesions. Numbers shown here represent lesions.

		Pathology		
		Malignant	Benign	**Total**
Clinical Diagnosis	Malignant	18	11	29
	Benign	0	**1**	1
	Total	18	12	30

		Pathology		
		Malignant	Benign	**Total**
Spectral Diagnosis	Malignant	18	6	24
	Benign	0	**6**	6
	Total	18	12	30